

## Enhanced Thermoelectric Performance of ZnO-based Oxide Materials

Michitaka OHTAKI\*, Shinichirou SHIGE\*\*,  
and Sayaka MAEHARA\*\*

\*Faculty of Engineering Sciences, Kyushu University;  
CREST, Japan Science and Technology Agency

Fax: 81-92-583-7465, e-mail: ohtaki@mm.kyushu-u.ac.jp

\*\*Interdisciplinary Graduate School of Engineering Sciences, Kyushu University

The thermoelectric properties were investigated for Al-doped zinc oxide sintered in the presence of void forming agents (VFA) such as small organic polymer particles of several hundreds nanometers in size. The sintered samples were revealed to have a number of closed pores (nanovoids) of 50-170 nm in diameter within the densified ZnO matrix. The samples showed marked enhancement in the thermopower, resulting in large negative maxima at the temperature range around 400-600 °C. On the other hand, the formation of the nanovoids scarcely influences the electrical conductivity if the size of VFA is sufficiently small. Although the reduction of the thermal conductivity is also fairly small, the enhanced thermopower coupled with the virtually unchanged electrical conductivity results in a considerable improvement in the power factor with the maximum value of  $40 \times 10^{-4} \text{ W/mK}^2$ , being twice as large as that of the completely dense sample without addition of VFA. The  $ZT$  value thereby exceeds 0.4, and the operation temperature range markedly expands toward the lower temperatures.

Key words: zinc oxide, nanostructure, phonon scattering, thermal conductivity, thermoelectric material

### 1. INTRODUCTION

Efficient energy utilization is one of the most important issues for sustainable future of human society. It is said that more than 60% of the primary energy supply is wasted as heat during its conversion, transfer, storage, and usage. Recovery of the waste heat energy has many difficulties, because the waste heat is diluted spatially and degraded in quality (low exergie). Thermoelectric power generation is expected as the "energy recycling" technology that can convert the vastly dispersed thermal energy directly to electrical energy. A solid element consisting of a pair of p- and n-type semiconductors operating over a temperature difference generates the thermoelectromotive force and hence electricity via the Seebeck effect of the semiconductor materials. Performance of thermoelectric materials is hence evaluated by the figure of merit defined as  $Z = S^2\sigma/\kappa$ , where  $S$  is the Seebeck coefficient,  $\sigma$  is the electrical conductivity, and  $\kappa$  is the thermal conductivity. Thermoelectric materials having been used in practical are intermetallic compounds such as  $\text{Bi}_2\text{Te}_3$ ,  $\text{PbTe}$ , and  $\text{Si-Ge}$  alloys. However, these materials have several shortcomings such as poor thermal durability, high toxicity, and high cost of the constituting elements. We have started pioneering work on oxide thermoelectric materials, which have many advantages in terms of environmental issues.

We have already reported that  $\text{Zn}_{0.98}\text{Al}_{0.02}\text{O}$  has exceedingly high thermoelectric performance compared to other oxides<sup>1</sup>. The addition of  $\text{Al}_2\text{O}_3$  to ZnO significantly enhances  $\sigma$ , retaining the moderate  $S$ . The power factor,  $S^2\sigma$ , which evaluates the electrical component of the thermoelectric performance, is consequently very large for  $\text{Zn}_{0.98}\text{Al}_{0.02}\text{O}$ . Unfortunately, however, the ZnO-based oxides showed the unfavorably high  $\kappa$ , which limit its  $Z$  value to insufficient level<sup>2</sup>. The lattice thermal conductivity

( $\kappa_{\text{ph}}$ ) is the principal component of  $\kappa$  of the oxides. If phonon scattering centers can be effectively introduced without scattering charge carriers, the  $Z$  values of the materials will be greatly improved. There have been many attempts to reduce  $\kappa_{\text{ph}}$ , because this is one of the principal issues in developing better thermoelectric materials<sup>3</sup>. Such attempts include forming void solutions (point defects)<sup>4</sup>, dispersing small particles as inert inclusions<sup>3,6</sup>, and using ultrafine powders in order to enhance phonon scattering at grain boundaries<sup>7</sup>. Porous structures have also been examined, but in general porous structures result in severe reduction in  $\sigma$ , overwhelming suppression in  $\kappa$  thereby attained<sup>8</sup>. However, incorporation of nanosized pores (nanovoids) into continuous dense matrices has not yet been experimentally investigated. In this work, suppression of high  $\kappa$  of  $\text{Zn}_{0.98}\text{Al}_{0.02}\text{O}$ , which is the best n-type oxide thermoelectric material so far, was investigated on microstructure control aiming at enhancement of phonon scattering.

### 2. EXPERIMENTAL

Samples of  $\text{Zn}_{0.98}\text{Al}_{0.02}\text{O}$  (hereafter abbreviated as ZnAl) were prepared by solid state reaction from commercially purchased ZnO and  $\gamma\text{-Al}_2\text{O}_3$  obtained by hydrolyzing aluminum isopropoxyde. Formation of solid solutions ( $\text{Zn}_{0.9}\text{M}_{0.1})_{0.98}\text{Al}_{0.02}\text{O}$  ( $\text{M} = \text{Mg}, \text{Ni}$ ) was carried out by partial substitution by MgO or NiO for ZnO. The starting powders were mixed and pulverized in nylon-lined ball mill for 24 h. The powder mixture was pressed into a pellet and sintered at 1400 °C for 10 h in air. Samples containing inclusions of other oxide particles  $\text{MO}_x$  ( $\text{ZnAl}+\text{MO}_x$ ) were prepared by adding fine powders of  $\text{ZrO}_2$  and  $\text{Y}_2\text{O}_3$  to the ZnAl powder prepared beforehand. One-pot sintering with  $\text{ZrO}_2$  inclusions was also carried out by mixing the raw materials at once ( $\text{ZnO}$ ,  $\gamma\text{-Al}_2\text{O}_3$ , and  $\text{ZrO}_2$  particles) as

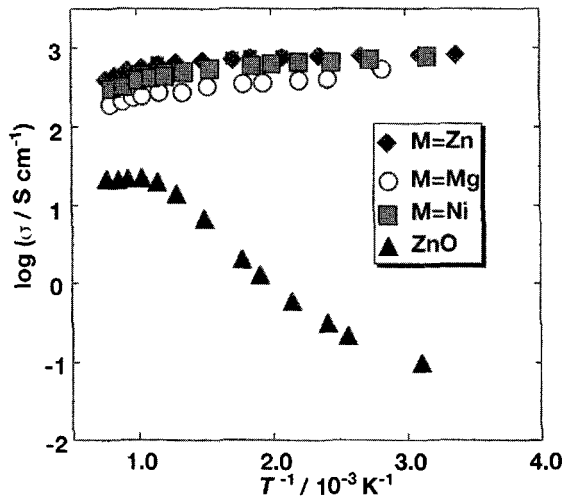


Fig. 1. The electrical conductivity of ZnO-based solid solutions ( $\text{Zn}_{0.9}\text{M}_{0.1}\text{Al}_{0.98}\text{O}$  ( $\text{M} = \text{Mg}, \text{Ni}$ )).

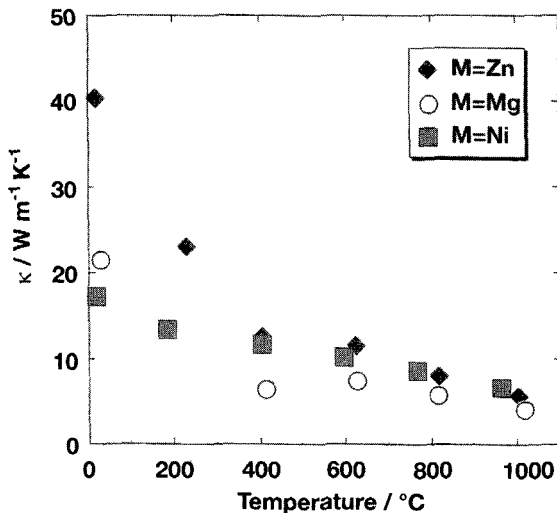


Fig. 2. The thermal conductivity of ZnO-based solid solutions ( $\text{Zn}_{0.9}\text{M}_{0.1}\text{Al}_{0.98}\text{O}$  ( $\text{M} = \text{Mg}, \text{Ni}$ )).

the starting mixture before sintering ( $\text{Zn}+\text{Al}+\text{ZrO}_2$ ). For Nanoporous ZnAl, 10 wt% of polymethylmethacrylate (PMMA) polymer beads ( $d_{\text{ave}} = 150 \text{ nm} - 1.8 \mu\text{m}$ ) was added to the starting mixture as void forming agent (VFA). Measurements of  $\sigma$  and  $S$  were simultaneously carried out in air, from room temperature up to  $1000 \text{ }^\circ\text{C}$ . The thermal conductivity was determined from the thermal diffusivity and the specific heat capacity measured by the laser flash technique on an ULVAC TC-7000.

### 3. RESULTS AND DISCUSSION

#### 3.1 Solid solution

The electrical conductivity of the solid solutions ( $\text{Zn}_{0.9}\text{M}_{0.1}\text{Al}_{0.98}\text{O}$  ( $\text{M} = \text{Mg}, \text{Ni}$ )) is shown in Fig. 1. The  $\sigma$  value of neat ZnAl was as extremely high as  $500 \text{ S/cm}$  at room temperature, its behavior being metallic with a gradual fall with increasing temperature. Compared to neat Zn-Al, a noticeable decrease in  $\sigma$  can be seen for the solid solution samples, yet the metallic

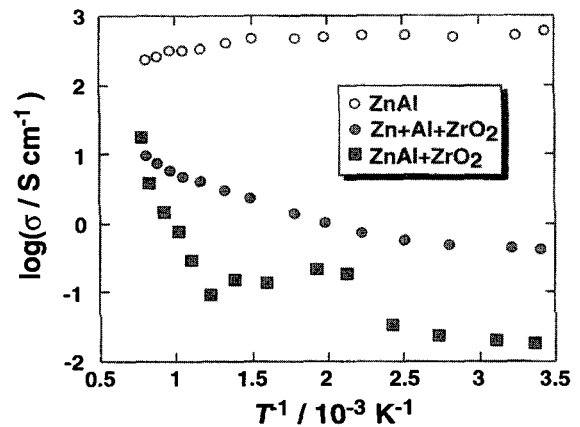


Fig. 3. The electrical conductivity of ZnAl dispersed with  $\text{ZrO}_2$  inclusions.

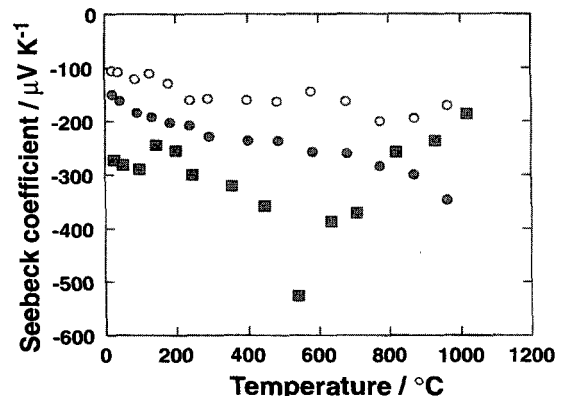


Fig. 4. The Seebeck coefficient of ZnAl dispersed with  $\text{ZrO}_2$  inclusions. The plot symbols are as the same as those in Fig. 3.

behavior being retained. The Seebeck coefficient was negative, indicating the n-type conduction, and the absolute values increased with temperature for all samples. The  $S$  value showed almost negligible changes by making solid solutions. Formation of solid solution with MgO and NiO achieved marked reduction of the thermal conductivity particularly at room temperature. The  $\kappa$  reduction was more significant for  $\text{M} = \text{Mg}$ , which is the lighter element than Zn. However, The power factors of the solid solutions were lower than that of ZnAl except near room temperature. The Hall measurement at room temperature revealed a considerable decrease in the carrier mobility for the solid solutions. Consequently, the figure-of-merit of the solid solutions stayed lower than that of ZnAl despite successful suppression of  $\kappa$ .

#### 3.2 Particle dispersion

Dispersion of other oxide particles  $\text{MO}_x$  largely reduced  $\sigma$  and changed the behavior into semiconducting. The serious reduction in  $\sigma$  was due to a roughly porous structure of the sintered samples. Moreover, the XRD study revealed a byproduct in  $\text{ZnAl}+\text{Y}_2\text{O}_3$  as the third phase, whereas no byproduct was found in  $\text{ZnAl}+\text{ZrO}_2$ . In addition, as for the samples dispersing  $\text{MO}_x$ , a small amount of spinel phase

ZnAl<sub>2</sub>O<sub>4</sub> usually coexisting in ZnAl was undetected. The serious suppression of  $\sigma$  for the ZnAl+ZrO<sub>2</sub> samples was significantly circumvented by one-pot sintering (Zn+Al+ZrO<sub>2</sub>).

Intense negative maxima of  $S$  were observed for the samples with porous structure. Such a large enhancement in  $S$  appears to be characteristic of porous oxide materials<sup>2</sup>.

Dispersion of the ZrO<sub>2</sub> inclusions with one-pot sintering successfully suppressed about 60% of the phonon thermal conductivity  $\kappa_{ph}$  of the neat ZnAl at room temperature. However, recovery of  $\sigma$  by one-pot sintering was still insufficient. As a result, the substantially low power factor counteracted the decrease in  $\kappa$ , and consequently lowered the figure of merit compared to ZnAl. Since the ZnAl<sub>2</sub>O<sub>4</sub> spinel phase found in ZnAl disappeared for the samples with the ZrO<sub>2</sub> inclusions, ZrO<sub>2</sub> may inactivate the Al dopant and thereby possibly lowered the carrier concentration.

### 3.3 Nanoporous ZnO

The  $\sigma$  values of the nanoporous ZnAl sintered with PMMA beads of  $d_{ave} = 150 \text{ nm} - 1.8 \mu\text{m}$  as VFA are shown in Fig. 5. The samples with VFA of  $d_{ave} = 430 \text{ nm}$  and  $1.8 \mu\text{m}$  exhibited serious suppression in  $\sigma$ , with changing the behavior to semiconducting. However, the sample with VFA of  $d_{ave} = 150 \text{ nm}$  retained almost the same values of the electrical conductivity as the neat ZnAl. The samples with VFA of  $d_{ave} = 430 \text{ nm}$  and  $1.8 \mu\text{m}$  yielded relative density of 90%, while 150nm VFA resulted in 99% relative density; the high and metallic  $\sigma$  values of the sample would be attributed to a dense ZnO matrix with small voids dispersed therein.

As seen in Fig. 6, the  $S$  values of the samples showed a behavior peculiar to the porous oxide structure; the thermopower showed intense negative maxima at about 500 - 700 °C, the peak temperature systematically decreasing with  $d_{ave}$  of VFA.

Although a huge thermopower was previously reported on porous Y<sub>2</sub>O<sub>3</sub>, only having been reported are those observed in vacuum<sup>9,10</sup>. The mechanism of the enhanced thermopower has been suggested as thermionic process in oxide pores; electrons are emitted from the pore walls towards the opposing inner surfaces of the pore. In the present study, the negative maxima in  $S$  were clearly observed in air. This maybe due to the voids smaller than the electron mean free path in air.

The Hall mobility  $\mu_H$  and the thermal conductivity measured at room temperature are plotted in Fig. 7 as a function of  $d_{ave}$  of VFA. With increasing  $d_{ave}$ , both  $\kappa$  and  $\mu_H$  markedly decreased. However, the extent of the reduction is much larger for  $\mu_H$  than for  $\kappa$ , indicating that the smaller pores are necessary for selective scattering of phonons rather than electrons. The reduction of  $\kappa$  for the smallest 150 nm VFA was moderate but significant. Consequently, the intense negative peak of  $S$  resulted in a large power factor of  $40 \times 10^{-4} \text{ W/mK}^2$  at 500 °C as shown in Fig. 8, achieving almost twice improvement at the peak value.

### 4. CONCLUSIONS

Suppression of high  $\kappa$  values of Zn<sub>0.98</sub>Al<sub>0.02</sub>O was investigated for making oxide solid solution, dispersing

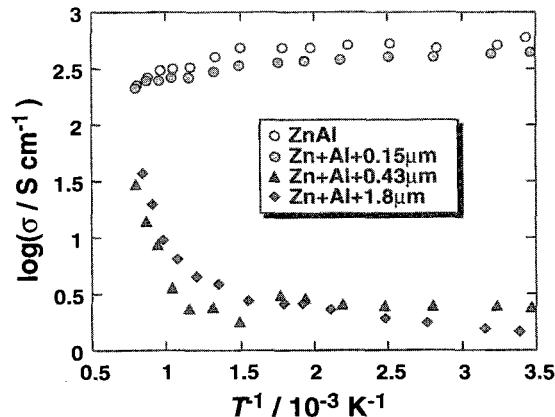


Fig. 5. The electrical conductivity of ZnAl sintered with PMMA beads of  $d_{ave} = 150 \text{ nm} - 1.8 \mu\text{m}$  as VFA.

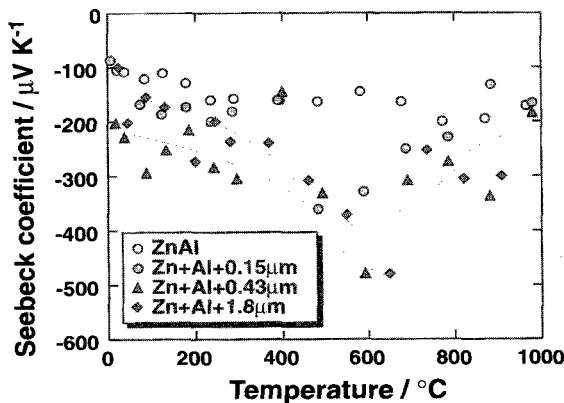


Fig. 6. The Seebeck coefficient of ZnAl sintered with PMMA beads of  $d_{ave} = 150 \text{ nm} - 1.8 \mu\text{m}$  as VFA.

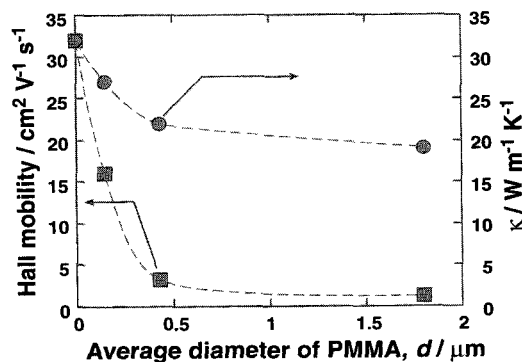


Fig. 7. The Hall mobility and the thermal conductivity at room temperature for ZnAl sintered with PMMA beads of  $d_{ave} = 150 \text{ nm} - 1.8 \mu\text{m}$  as VFA.

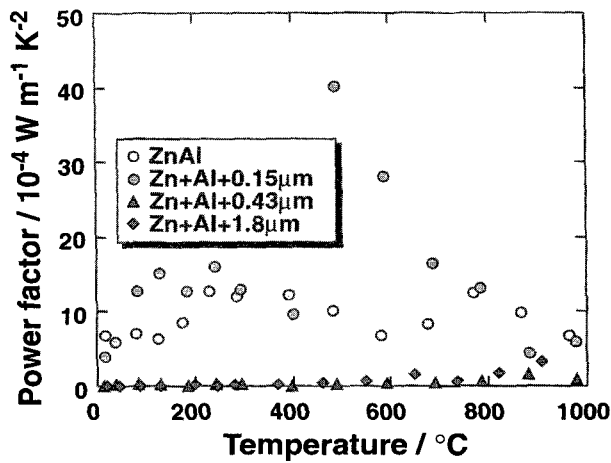


Fig. 8. The power factor of ZnAl sintered with PMMA beads of  $d_{ave} = 150 \text{ nm} - 1.8 \text{ }\mu\text{m}$  as VFA.

oxide particle inclusion, and making nanoporous structures, aiming at selective enhancement of phonon scattering. Dispersion of oxide inclusions such as  $\text{ZrO}_2$  with one-pot sintering successfully suppressed about 60% of  $\kappa_{ph}$ . The porous ZnAl prepared by addition of PMMA polymer beads also reduced about 30% of  $\kappa_{ph}$ . Nevertheless, a substantial decrease in  $\sigma$  lowered the power factor of the inclusion samples. However, nanopores or nanovoids dispersed within the densely sintered matrix, which situation is qualitatively the same as that of one of the possible ideal structures: a continuum (single crystal) with very small pores dispersed therein.

The PMMA VFA formed small voids within densely sintered ZnO matrix. With 150 nm VFA,  $\sigma$  and  $\kappa$  almost unchanged but  $S$  was drastically enhanced. Consequently, a power factor of  $40 \times 10^{-4} \text{ W/mK}^2$  was attained at 500 °C, leading to higher  $ZT$ . As a reason of the enhanced  $S$ , theomionic process in the nanovoids of 50-170 nm is suggested.

Changes in the size of particles or voids, and optimization of doping are expected to improve the matrix properties.

## 5. REFERENCES

- [1] M. Ohtaki, T. Tsubota, K. Eguchi, and H. Arai, *J. Appl. Phys.*, **79**(3), 1816-1817 (1996).
- [2] T. Tsubota, M. Ohtaki, K. Eguchi, and H. Arai, *J. Mater. Chem.*, **8** (2), 409-412 (1998).
- [3] D. M. Rowe, Ed.: *CRC Handbook of Thermoelectrics*, CRC Press, Inc., Boca Raton (1995).
- [4] M. Ohtaki, T. Tsubota, and K. Eguchi, *Proc. 17th Int. Conf. Thermoelectrics*, pp. 610-613 (1998).
- [5] C. B. Vining, *Mater. Res. Soc. Symp. Proc.*, **234**, pp. 95-104 (1991).
- [6] J. W. Vandersande, J.-P. Fleurial, N. Scoville, and J. L. Rolfe, *Proc. 12nd Int. Conf. Thermoelectrics*, pp. 11-14 (1993).
- [7] S. Katsuyama, Y. Takagi, M. Ito, K. Majima, H. Nagai, H. Sakai, K. Yoshimura, and K. Kosuge, *J. Appl. Phys.*, **92**(3), 1391-1398 (2002).
- [8] M. Ohtaki and S. Shige, *21st Int. Conf. Thermoelectrics*, unpublished (2002).

*Thermoelectrics*, unpublished (2002).

[9] K. Koumoto, *et al.*, *Proc. 16th Int. Conf. Thermoelectrics*, p. 467-470 (1997).

[10] K. Koumoto, W. S. Seo, and S. Ozawa, *Appl. Phys. Lett.*, **71**(11), 1475-1476 (1997).

(Received October 13, 2003; Accepted January 16, 2004)